

## ARTICLE OPEN



# Expansion of the high field-boosted superconductivity in $\text{UTe}_2$ under pressure

Sheng Ran<sup>1,2,3</sup>✉, Shanta R. Saha<sup>1,2</sup>, I-Lin Liu<sup>1,2</sup>, David Graf<sup>4</sup>, Johnpierre Paglione<sup>1,2</sup> and Nicholas P. Butch<sup>1,2</sup>✉

Magnetic field-induced superconductivity is a fascinating quantum phenomenon, whose origin is yet to be fully understood. The recently discovered spin-triplet superconductor,  $\text{UTe}_2$ , exhibits two such superconducting phases, with the second one reentering in the magnetic field of 45 T and persisting up to 65 T. More surprisingly, in order to induce this superconducting phase, the magnetic field has to be applied in a special angle range, not along any high symmetry crystalline direction. Here we investigated the evolution of this high-field-induced superconducting phase under pressure. Two superconducting phases merge together under pressure, and the zero resistance persists up to 45 T, the field limit of the current study. We also reveal that the high-field-induced superconducting phase is completely decoupled from the first-order field-polarized phase transition, different from the previously known example of field-induced superconductivity in URhGe, indicating superconductivity boosted by a different pairing mechanism.

npj Quantum Materials (2021)6:75; <https://doi.org/10.1038/s41535-021-00376-9>

## INTRODUCTION

The recent evidence for spin-triplet superconductivity in  $\text{UTe}_2$  has opened an avenue for the study of topological superconductivity<sup>1</sup>. The superconducting state of  $\text{UTe}_2$  closely resembles that of ferromagnetic superconductors, but the normal state is paramagnetic and shows no indication of magnetic ordering<sup>2–4</sup>. Spin-triplet pairing is strongly indicated by the extremely large, anisotropic upper critical field  $H_{c2}$ <sup>1,5</sup>, nodes on the superconducting gap<sup>6,7</sup>, and the temperature-independent NMR Knight shift in the superconducting state<sup>8,9</sup>. The superconducting order parameter comprises two components and breaks time-reversal symmetry<sup>10,11</sup>. A nontrivial topology is suggested by the observation of chiral in-gap bound states by scanning tunneling spectroscopy<sup>12</sup>.

Even more striking,  $\text{UTe}_2$  hosts two independent field-induced superconducting phases<sup>13–16</sup>, with the higher-field phase reentering at a high magnetic field of 45 T and persisting up to 65 T when the magnetic field is aligned over a limited angular range about the normal direction of the (011) plane. The quasi-two-dimensional Fermi surface revealed by band structure calculations and photoemission measurements<sup>17–19</sup>, as well as the lack of a ferromagnetic ground state, has led to suggestions that the field-induced superconductivity in  $\text{UTe}_2$  is due to reduced dimensionality instead of magnetic fluctuations<sup>20,21</sup>: a magnetic field applied parallel to quasi 2D conducting layers will stabilize superconductivity when the magnetic energy reaches the hopping amplitude between the conducting layers<sup>20,22</sup>.

In this work, we investigate the evolution of the magnetic field-induced superconducting phases in  $\text{UTe}_2$  as pressure is applied to samples oriented specifically along the off-axis angle which stabilizes the high-field phase. Over a range of pressures near 1 GPa, the two different superconducting phases merge together, and the electrical resistance remains zero up to at least 45 T, a remarkably large value for a superconductor with a 3 K critical temperature. The high-field-induced superconducting phase is

completely decoupled from the first-order transition to a field-polarized state, suggesting that magnetic fluctuations may not be crucial to this reentrant superconductivity. At pressures exceeding the critical pressure at which metamagnetic phase transition extrapolates to zero magnetic field, we observe features with the same temperature dependence as the high-field-induced superconducting phase, further investigation of which might shed light on the mechanism reentrant superconductivity.

## RESULTS AND DISCUSSION

### Pressure-magnetic field phase diagram

To characterize the evolution of the high-field-induced superconducting phase under pressure, we performed complementary measurements of electrical resistance  $R$  and tunnel diode oscillator (TDO) frequency  $\Delta f$ , which is sensitive to the change of both electrical resistance and magnetic susceptibility. Two samples were studied for which the magnetic field was applied  $\sim 25^\circ$  and  $30^\circ$ , respectively, away from the  $b$  axis toward  $c$ . At ambient pressure, three distinct phases were observed as shown in Fig. 1: a field-polarized state FP with greatly enhanced magnetization and resistance<sup>13,15,16,23</sup>; the low-field superconducting phase,  $\text{SC}_{\text{PM}}$ , coexisting with the paramagnetic state; and the high-field-induced superconducting phase,  $\text{SC}_{\text{FP}}$ , existing inside the field-polarized state. The criteria used to infer critical magnetic field for each phase are explained in the Supplementary Information (see Supplementary Figs. 4–7).

Absent in this field configuration is another field-induced superconducting phase that is observed on the low-field side of the metamagnetic field  $H_{\text{FP}}$  when the magnetic field is applied along the  $b$  axis. For magnetic field along the  $b$  axis, applied pressure suppresses the metamagnetic field to zero at 1.5 GPa and forces a phase transition inside the paramagnetic state at a crossover pressure  $P_x$ , from  $\text{SC}_{\text{PM1}}$  to  $\text{SC}_{\text{PM2}}$ , in zero magnetic field at  $\sim 1$  GPa<sup>24</sup>. Recent symmetry analysis indicates that the  $\text{SC}_{\text{PM1}}$

<sup>1</sup>Maryland Quantum Materials Center, Department of Physics, University of Maryland, College Park, MD, USA. <sup>2</sup>NIST Center for Neutron Research, National Institute of Standards and Technology, Gaithersburg, MD, USA. <sup>3</sup>Department of Physics, Washington University in St. Louis, St. Louis, MO, USA. <sup>4</sup>National High Magnetic Field Laboratory, Florida State University, Tallahassee, FL, USA. ✉email: [rans@wustl.edu](mailto:rans@wustl.edu); [nbutch@umd.edu](mailto:nbutch@umd.edu)

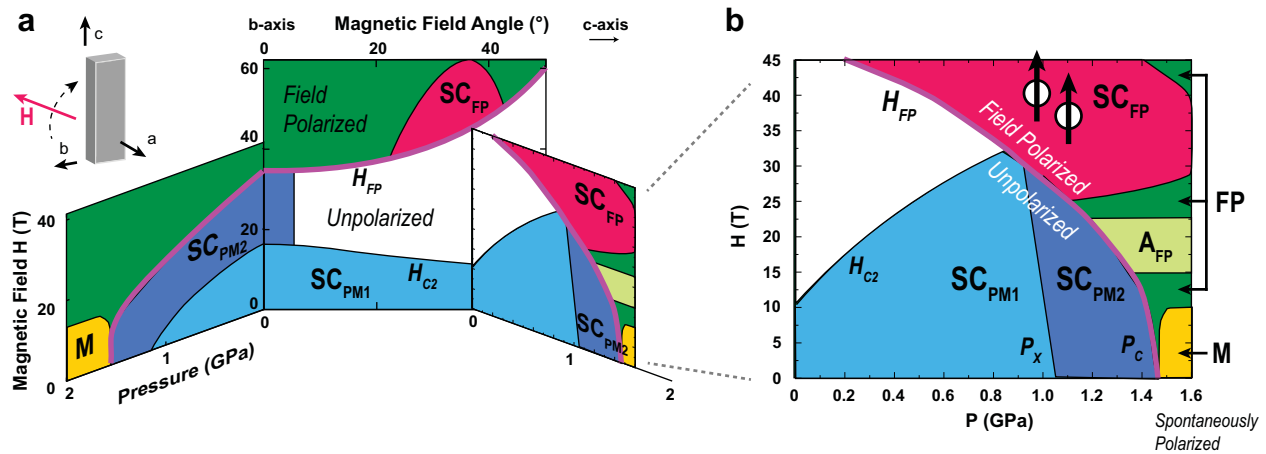


**Fig. 1 The stability of superconducting and magnetic phases of  $\text{UTe}_2$ .** **a** The zero-field superconducting phase  $\text{SC}_{\text{PM1}}$  exhibits a strongly direction-dependent upper critical field  $H_{\text{C2}}$ . Along the crystallographic  $b$  axis, the reentrant superconducting phase  $\text{SC}_{\text{PM2}}$  is stabilized up to a first-order magnetic transition at  $H_{\text{FP}}$ , above which exists a magnetically polarized phase FP. Applied pressure uniformly suppresses all field scales and  $H_{\text{FP}}$  bounds superconductivity up to a critical pressure  $P_{\text{C}}$ . **b** For a magnetic field oriented between 25 and 30° between the  $b$ - and  $c$  axes, the high-field reentrant superconductivity  $\text{SC}_{\text{FP}}$  stabilizes in the FP phase. Applied pressure enhances  $\text{SC}_{\text{PM1}}$ , which meets a decreasing  $H_{\text{FP}}$  at a crossover region  $P_{\text{x}}$ . Here,  $\text{SC}_{\text{PM1}}$  transitions to  $\text{SC}_{\text{PM2}}$ , which survives up to  $P_{\text{C}}$ , where it is replaced by magnetic order M. Below  $P_{\text{x}}$ ,  $H_{\text{FP}}$  is a lower bound on  $\text{SC}_{\text{FP}}$ , but above  $P_{\text{x}}$  the two are decoupled and  $\text{SC}_{\text{FP}}$  survives beyond  $P_{\text{C}}$ . An anomaly  $A_{\text{FP}}$ , suggestive of Landau-level superconductivity, emerges above  $P_{\text{C}}$ . The phase diagram is based on the resistance data shown in Fig. 2.

phase has a two-component order parameter while the order parameter of  $\text{SC}_{\text{PM2}}$  phase only has one component<sup>11</sup>. Our measurements in this study do not exhibit any field-induced features<sup>24</sup>, so we infer that the  $\text{SC}_{\text{PM1}}$ - $\text{SC}_{\text{PM2}}$  boundary is nearly vertical in the  $H$ - $P$  plane. At pressures exceeding 1.5 GPa, long-range magnetic order is stabilized<sup>25–28</sup>, whose features have been interpreted in terms of both ferromagnetism<sup>24,25</sup> and antiferromagnetism<sup>27</sup>. Without an unambiguous experimental proof of the nature of this phase, in this study we label it as a magnetically ordered phase, M.

The pressure-magnetic field phase diagram for the magnetic field in this angle range is summarized in Fig. 1. All three phases manifest clear evolution under pressure, as seen in  $R$  and  $\Delta f$  in Fig. 2. The metamagnetic field is monotonically suppressed by the applied pressure, similar to the behavior for field along  $b$ <sup>24</sup>, although it starts at a higher value. The metamagnetic field vanishes at a critical pressure  $P_{\text{C}}$  between 1.47 and 1.54 GPa, giving rise to a spontaneously polarized state in zero magnetic field beyond this pressure. Over the entire pressure range, both  $R$  and  $\Delta f$  change discontinuously on passing through the metamagnetic field in the normal state, implying that it maintains the first-order metamagnetic transition observed at ambient pressure<sup>15,23,29</sup>.

Upon initial increase of the pressure, the stability of both superconducting phases is enhanced: the upper critical field of  $\text{SC}_{\text{PM}}$ ,  $H_{\text{C2}}$ , increases, and the critical onset field of  $\text{SC}_{\text{FP}}$ ,  $H_{\text{I}}$ , which coincides with the metamagnetic field, decreases. In an intermediate crossover pressure range, the phase boundary between  $\text{SC}_{\text{PM}}$  and  $\text{SC}_{\text{FP}}$  is no longer visible in the electrical resistance; this remains zero up to 45 T at base temperature, which is noteworthy as it is the largest DC magnetic field currently available to experiment (Fig. 3). As the pressure further increases, the upper critical field of  $\text{SC}_{\text{PM}}$  is limited by the metamagnetic field and decreases, but the critical onset field of  $\text{SC}_{\text{FP}}$  starts to increase, and the two superconducting phases are no longer connected. When the metamagnetic field vanishes,  $\text{SC}_{\text{PM}}$  is suppressed completely.

Subtle differences between the electrical resistance and TDO samples highlight the effects of their slight angular offset (Fig. 2). As the TDO sample sits at a slightly larger angle away from the  $b$  axis, the upper critical field of  $\text{SC}_{\text{PM}}$  has a smaller value and the critical onset field of  $\text{SC}_{\text{FP}}$  has a larger value at ambient pressure. The  $\text{SC}_{\text{PM}}$  and  $\text{SC}_{\text{FP}}$  phases remain connected over a much smaller

pressure range. Similarly, the field-polarized state starts above a higher magnetic field because the metamagnetic field is larger, but it is suppressed faster upon increasing pressure and vanishes also at  $P_{\text{C}}$ .

The discontinuous nature of the metamagnetic transition at  $H_{\text{FP}}$  is conspicuous in the resistance data (Fig. 3). At low pressures, a sharp upward jump marking the FP phase boundary is replaced at low temperatures by a sharp downward jump marking the  $\text{SC}_{\text{FP}}$  phase boundary. An additional hallmark of first-order transitions, namely field-hysteresis is also readily apparent. In the intermediate pressure range,  $H_{\text{FP}}$  limits the lower-field superconducting phase  $\text{SC}_{\text{PM}}$ . Here, the transitions associated with  $H_{\text{FP}}$  are again hysteretic. Interestingly, the decoupled  $\text{SC}_{\text{FP}}$  phase appears to also exhibit some small hysteresis, the origin of which may be associated with details of the field reentrance. These features are consistent at all measured pressures.

These details reveal important points about the relationships between the many electronic phases. The low- and high-field superconducting phases always exist on opposite sides of the metamagnetic transition  $H_{\text{FP}}$ , upon which Fermi surface reconstruction has been suggested based on thermoelectric power and Hall effect measurements<sup>23,30,31</sup>. In addition, in the low-pressure range,  $\text{SC}_{\text{FP}}$  only appears on the high-field side of the metamagnetic field (Fig. 2a, b), while  $\text{SC}_{\text{PM}}$  only exists at fields lower than the metamagnetic field. The role of the metamagnetic field switches in the intermediate pressure range, where the metamagnetic field truncates the low-field phase  $\text{SC}_{\text{PM}}$ . This behavior is apparent in both panels of Fig. 2c, where the high-temperature part of the upper critical field of  $\text{SC}_{\text{PM}}$  curve rises rapidly as temperature decreases, extrapolating to field values far higher than the metamagnetic field, but then, as soon as the upper critical field of  $\text{SC}_{\text{PM}}$  coincides with the metamagnetic field, the behavior suddenly changes and the upper critical field of  $\text{SC}_{\text{PM}}$  becomes almost temperature-independent down to low temperatures. Taken together, these facts imply that the  $\text{SC}_{\text{PM}}$  and  $\text{SC}_{\text{FP}}$  phases separated by the metamagnetic transition might have different superconducting pairings that are unique to PM and FP, respectively. It is particularly striking that both low- and high-field superconducting phases look like they would cover much larger ranges of the field were they not limited by the metamagnetic field.

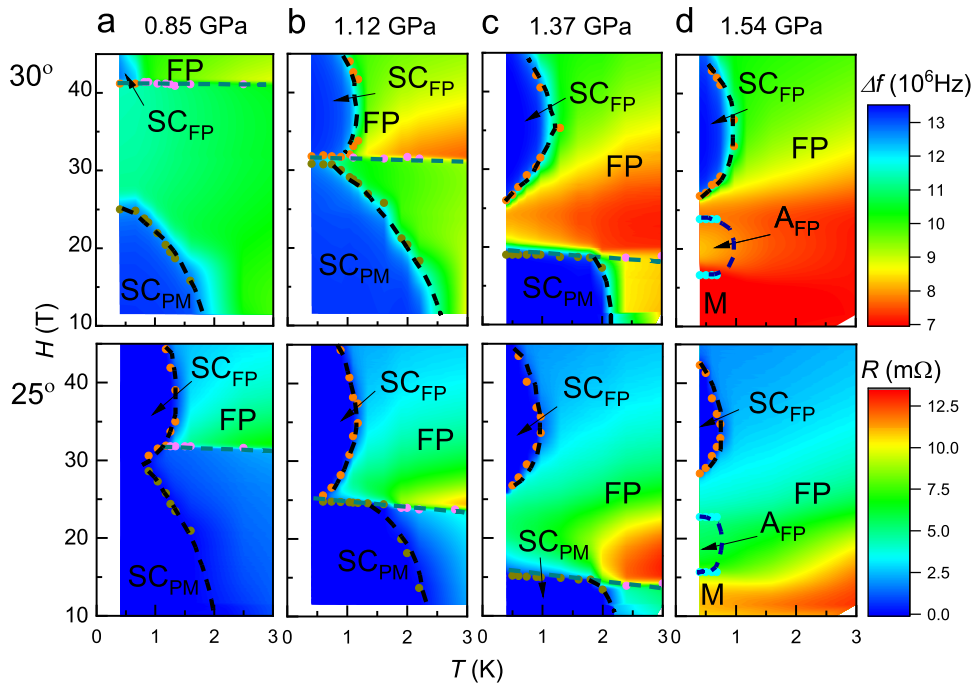


**Fig. 2 High-field TDO frequency and resistance at different pressures.** TDO frequency is sensitive to the change of both electrical resistance and magnetic susceptibility of the sample. Magnetic field is applied at  $30^\circ$  from  $b$  axis toward  $c$  axis for TDO measurement, and  $25^\circ$  from  $b$  axis toward  $c$  axis for resistance measurement. **a** In the low-pressure region,  $H_{FP}$  serves as a lower bound to  $SC_{FP}$ , whose dome is cut off discontinuously. **b** At crossover pressures  $P_x$ ,  $H_{FP}$  falls approximately between  $SC_{FP}$  and  $SC_{PM}$ , whose ranges of stability would otherwise overlap. **c** Above  $P_x$ ,  $H_{FP}$  serves as the upper field limit for  $SC_{PM}$ . **d** Above  $P_c$ , long-range ordered magnetism  $M$  sets in while  $SC_{FP}$  survives and the anomalous feature  $A_{FP}$  emerges as a local maximum in  $\Delta f$ . Solid dots are from experimental data, dashed lines are guide for the eye. Note that TDO and resistance measurements are performed for slightly different magnetic field direction, which leads to the slightly different phase diagrams for each pressure.

In the high-pressure range, the critical onset field of  $SC_{FP}$  and the metamagnetic field are well separated, by more than 20 T. This is crucial for the understanding of the pairing mechanism of the  $SC_{FP}$  phase. In the case of URhGe, the reentrance of superconductivity can be explained in terms of ferromagnetic fluctuations parallel to the direction of the magnetic field. In that case, reentrant SC occurs in the vicinity of the magnetic critical field. In  $UTe_2$  at low pressure, the  $SC_{FP}$  phase resembles somewhat the reentrant phase in URhGe, leading to the speculation that magnetic fluctuations are also responsible for reentrant superconductivity in  $UTe_2$ . However, here we show clearly that the  $SC_{FP}$  phases can exist in the region far away from the field-polarized phase line, indicating a possibility scenario that magnetic fluctuations are not responsible for the pairing mechanism. Future experiments to investigate magnetic fluctuations in the vicinity of the  $SC_{FP}$  phase at pressure above 1.3 GPa will potentially shed light on the pairing mechanism.

### Anomaly in the high-pressure region

A striking characteristic of the high-pressure FP phase is the emergence of additional features in the field range between the  $M$  and  $SC_{FP}$  phases. These anomalies, denoted  $A_{FP}$ , are pronounced in the  $\Delta f$  data, and noticeable in  $R$  data (Fig. 4). It is not clear whether these anomalies correspond to a thermodynamically distinct phase. In order to trace the evolution of these anomalies, we introduced criteria to define the boundaries as shown in the Supplementary Materials. These anomalies exhibit a clear temperature dependence below 1.2 K. This notable similarity to the temperature dependence of  $SC_{FP}$  suggests that  $A_{FP}$  is a closely related phenomenon, with a similar energy scale to that of the superconductivity. This distinguishes  $A_{FP}$  from the zero-field magnetically ordered phase  $M$ , which has a higher-temperature

ordering temperature relative to superconductivity, that continues to increase with applied pressure.

An exciting possibility is that  $A_{FP}$  is a precursor to superconductivity. Previous theoretical studies have shown that in extreme magnetic field Landau levels will have a dramatic influence on the low-temperature behavior of the upper critical field<sup>32–34</sup>. Indeed, a more recent theoretical study indicates that  $SC_{FP}$  might be a form of superconductivity that is enhanced by high-field Landau quantization of the conduction electrons<sup>35</sup>. Therefore,  $A_{FP}$  and  $SC_{FP}$  may actually be the same superconducting phase occurring at different Landau levels, analogous to Shubnikov-de Haas oscillations. A challenge to this interpretation is that  $A_{FP}$  is not accompanied by a zero-resistance state (Fig. 3a), but a plausible explanation for this is that  $A_{FP}$  is actually partially superconducting due to the effects of energy-level broadening are stronger at the lower field. Based on the inverse-field periodicity of  $A_{FP}$ , the next Landau level will be centered at  $\sim 100$  T, achieving zero resistance at magnetic fields as low as 90 T, which is practically achievable using the strongest available nondestructive pulsed magnet systems.

## METHODS

### Crystal synthesis

Single crystals of  $UTe_2$  were synthesized by the chemical vapor transport method using iodine as the transport agent. Elements of U and Te with atomic ratio 2:3 were sealed in an evacuated quartz tube, together with  $3 \text{ mg/cm}^3$  iodine. The ampoule was gradually heated up and hold in the temperature gradient of 1060/1000 °C for 7 days, after which it was furnace cooled to room temperature. The crystal structure was determined by X-ray powder diffraction using a Rigaku X-ray diffractometer with  $\text{Cu-K}\alpha$  radiation. Crystal orientation was determined by Laue X-ray diffraction performed with a Photonic Science X-ray measurement system.

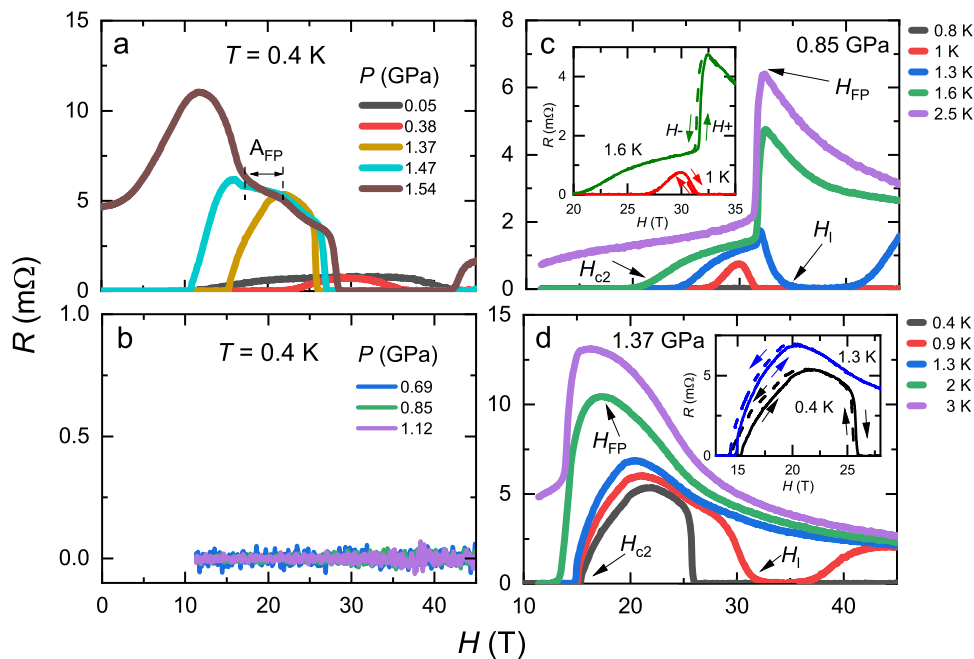


**Fig. 3 High-field magnetoresistance, showing phase boundaries at different pressures.** Magnetic field is applied at  $25^\circ$  from  $b$  axis toward  $c$  axis. **a** Pressure dependence of 0.4 K magnetoresistance, showing the sharpening of phase boundaries at higher pressures and emergence of high-pressure phase  $A_{FP}$ . **b** The resistance at pressures 0.69, 0.85, and 1.12 GPa is zero between 11 and 45 T at 0.4 K. Zero resistance persists to zero magnetic field at these pressure values. **c** For fields lower than  $H_{FP}$ , the superconducting transitions  $H_{C2}$  are broad, but  $H_{FP}$  is sharp. As shown in inset,  $H_{FP}$  is hysteretic, reflecting the 1st order transition, both at high temperatures in the FP phase and low temperature in the  $SC_{FP}$  phase. **d** Much sharper superconducting phase boundaries occur once  $H_{FP}$  limits  $SC_{FP}$ . As shown in inset, low-field phase boundaries are hysteretic and first order, as is the onset of  $SC_{FP}$ .

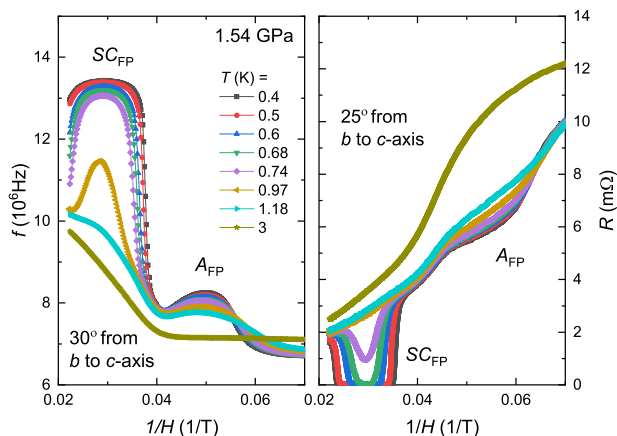


**Fig. 4 Additional anomalies emerge in the high-pressure region.**  $A_{FP}$  phase appears at 1.54 GPa in both TDO and resistance data, which have the same temperature dependence as  $SC_{FP}$  phase, indicating  $A_{FP}$  phase might be the precursor of superconductivity. Magnetic field is applied at  $30^\circ$  from  $b$  axis toward  $c$  axis for TDO measurement, and  $25^\circ$  from  $b$  axis toward  $c$  axis for resistance measurement.

### Measurement

Magnetoresistance and tunnel diode oscillator (TDO) measurements were performed at the National High Magnetic Field Laboratory, Tallahassee, using the 45-T hybrid magnet. A non-magnetic piston-cylinder pressure cell was used for measurements under pressure up to 1.57 GPa, with Daphne oil 7575 as the pressure medium. Pressure was calibrated at low temperatures by measuring the fluorescence wavelength of ruby, which has a known temperature and pressure dependence. The TDO technique uses an LC oscillator circuit biased by a tunnel diode whose resonant frequency is determined by the values of LC components, with the inductance  $L$  given by a coil that contains the sample under study; the

change of its electrical resistance and magnetic properties results in a change in resonant frequency. Identification of commercial equipment does not imply recommendation or endorsement by NIST. Error bars correspond to uncertainty of one standard deviation.

### DATA AVAILABILITY

The data that support the findings of this study are available from the corresponding author upon reasonable request.

Received: 24 March 2021; Accepted: 9 July 2021;  
Published online: 06 September 2021

### REFERENCES

- Ran, S. et al. Nearly ferromagnetic spin-triplet superconductivity. *Science* **365**, 684–687 (2019).
- Sundar, S. et al. Coexistence of ferromagnetic fluctuations and superconductivity in the actinide superconductor  $UTe_2$ . *Phys. Rev. B* **100**, 140502 (2019).
- Hutano, V. et al. Low-temperature crystal structure of the unconventional spin-triplet superconductor  $UTe_2$  from single-crystal neutron diffraction. *Acta Crystallogr. Sect. B* **76**, 137–143 (2020).
- Duan, C. et al. Incommensurate spin fluctuations in the spin-triplet superconductor candidate  $UTe_2$ . *Phys. Rev. Lett.* **125**, 237003 (2020).
- Aoki, D. et al. Unconventional superconductivity in heavy fermion  $UTe_2$ . *J. Phys. Soc. Jpn.* **88**, 043702 (2019).
- Metz, T. et al. Point-node gap structure of the spin-triplet superconductor  $UTe_2$ . *Phys. Rev. B* **100**, 220504 (2019).
- Bae, S. et al. Anomalous normal fluid response in a chiral superconductor  $UTe_2$ . *Nat. Commun.* **12**, 2644 (2021).
- Nakamine, G. et al. Superconducting properties of heavy fermion  $UTe_2$  revealed by  $^{125}\text{Te}$ -nuclear magnetic resonance. *J. Phys. Soc. Jpn.* **88**, 113703 (2020).
- Nakamine, G. et al. Anisotropic response of spin susceptibility in the superconducting state of  $UTe_2$  probed with  $^{125}\text{Te}$ -NMR measurement. *Phys. Rev. B* **103**, L100503 (2021).

10. Hayes, I. M. et al. Multicomponent superconducting order parameter in  $UTe_2$ . *Science* **373**, 797–801 (2021).
11. Shishidou, T., Suh, H. G., Brydon, P. M. R., Weinert, M. & Agterberg, D. F. Topological band and superconductivity in  $UTe_2$ . *Phys. Rev. B* **103**, 104504 (2021).
12. Jiao, L. et al. Chiral superconductivity in heavy-fermion metal  $UTe_2$ . *Nature* **579**, 523–527 (2020).
13. Ran, S. et al. Extreme magnetic field-boosted superconductivity. *Nat. Phys.* **15**, 1250–1254 (2019).
14. Knebel, G. et al. Field-reentrant superconductivity close to a metamagnetic transition in the heavy-fermion superconductor  $UTe_2$ . *J. Phys. Soc. Jpn.* **88**, 063707 (2019).
15. Knafo, W. et al. Magnetic-field-induced phenomena in the paramagnetic superconductor  $UTe_2$ . *J. Phys. Soc. Jpn.* **88**, 063705 (2019).
16. Knafo, W. et al. Comparison of two superconducting phases induced by a magnetic field in  $UTe_2$ . *Commun. Phys.* **4**, 40 (2021).
17. Miao, L. et al. Low energy band structure and symmetries of  $UTe_2$  from angle-resolved photoemission spectroscopy. *Phys. Rev. Lett.* **124**, 076401 (2020).
18. Xu, Y., Sheng, Y. & Yang, Y.-f. Quasi-two-dimensional fermi surfaces and unitary spin-triplet pairing in the heavy fermion superconductor  $UTe_2$ . *Phys. Rev. Lett.* **123**, 217002 (2019).
19. Ishizuka, J., Sumita, S., Daido, A. & Yanase, Y. Insulator-metal transition and topological superconductivity in  $UTe_2$  from a first-principles calculation. *Phys. Rev. Lett.* **123**, 217001 (2019).
20. Lebed, A. G. & Yamaji, K. Restoration of superconductivity in high parallel magnetic fields in layered superconductors. *Phys. Rev. Lett.* **80**, 2697–2700 (1998).
21. Mineev, V. P. Reentrant superconductivity in  $UTe_2$ . *JETP Lett.* **111**, 715–719 (2020).
22. Lebed, A. G. Restoration of superconductivity in high magnetic fields in  $UTe_2$ . *Mod. Phys. Lett. B* **34**, 2030007 (2021).
23. Miyake, A. et al. Metamagnetic transition in heavy fermion superconductor  $UTe_2$ . *J. Phys. Soc. Jpn.* **88**, 063706 (2019).
24. Lin, W.-C. et al. Tuning magnetic confinement of spin-triplet superconductivity. *npj Quantum Mater.* **5**, 68 (2020).
25. Ran, S. et al. Enhancement and reentrance of spin triplet superconductivity in  $UTe_2$  under pressure. *Phys. Rev. B* **101**, 140503 (2020).
26. Braithwaite, D. et al. Multiple superconducting phases in a nearly ferromagnetic system. *Commun. Phys.* **2**, 147 (2019).
27. Thomas, S. M. et al. Evidence for a pressure-induced antiferromagnetic quantum critical point in intermediate-valence  $UTe_2$ . *Sci. Adv.* **6**, eabc8709 (2020).
28. Aoki, D. et al. Multiple superconducting phases and unusual enhancement of the upper critical field in  $UTe_2$ . *J. Phys. Soc. Jpn.* **89**, 053705 (2021).
29. Imajo, S. et al. Thermodynamic investigation of metamagnetism in pulsed high magnetic fields on heavy fermion superconductor  $UTe_2$ . *J. Phys. Soc. Jpn.* **88**, 083705 (2019).
30. Niu, Q. et al. Fermi-surface instability in the heavy-fermion superconductor  $UTe_2$ . *Phys. Rev. Lett.* **124**, 086601 (2020).
31. Niu, Q. et al. Evidence of fermi surface reconstruction at the metamagnetic transition of the strongly correlated superconductor  $UTe_2$ . *Phys. Rev. Res.* **2**, 033179 (2020).
32. Gruenberg, L. W. & Gunther, L. Effect of orbital quantization on the critical field of type-II superconductors. *Phys. Rev.* **176**, 606–613 (1968).
33. Tešanović, Z., Rasolt, M. & Xing, L. Quantum limit of a flux lattice: superconductivity and magnetic field in a new relationship. *Phys. Rev. Lett.* **63**, 2425–2428 (1989).
34. Song, K. W. & Koshelev, A. E. Strong Landau-quantization effects in high-magnetic-field superconductivity of a two-dimensional multiple-band metal near the Lifshitz transition. *Phys. Rev. B* **95**, 174503 (2017).
35. Park, M. J., Kim, Y. B. & Lee, S. Geometric superconductivity in 3d Hofstadter butterfly. Preprint at <https://arxiv.org/abs/arXiv:2007.16205> (2020).

## ACKNOWLEDGEMENTS

We acknowledge D. Agterberg, G. S. Boebinger, A. E. Koshelev, A. Lebed, and V. P. Mineev for inspiring discussions. Research at the University of Maryland was supported by the National Institute of Standards and Technology (NIST), the US National Science Foundation (NSF) Division of Materials Research Award No. DMR-1610349, the US Department of Energy (DOE) Award No. DE-SC-0019154 (experimental investigations), and the Gordon and Betty Moore Foundation's EPIQS Initiative through Grant No. GBMF4419 (materials synthesis). Work performed at the National High Magnetic Field Laboratory, USA (NHMFL) was supported by NSF through NSF/DMR-1644779 and the State of Florida.

## AUTHOR CONTRIBUTIONS

N.P.B. and S.R. conceived and designed the study. S.R. and S.R.S. synthesized the single-crystalline samples. S.R., S.R.S., I.L. and D.G. performed the electrical resistivity and tunnel diode oscillator measurements. S.R., J.P. and N.P.B. analyzed the data and wrote the paper with everyone's contribution.

## COMPETING INTERESTS

The authors declare no competing interests.

## ADDITIONAL INFORMATION

**Supplementary information** The online version contains supplementary material available at <https://doi.org/10.1038/s41535-021-00376-9>.

**Correspondence** and requests for materials should be addressed to S.R. or N.P.B.

**Reprints and permission information** is available at <http://www.nature.com/reprints>

**Publisher's note** Springer Nature remains neutral with regard to jurisdictional claims in published maps and institutional affiliations.



**Open Access** This article is licensed under a Creative Commons Attribution 4.0 International License, which permits use, sharing, adaptation, distribution and reproduction in any medium or format, as long as you give appropriate credit to the original author(s) and the source, provide a link to the Creative Commons license, and indicate if changes were made. The images or other third party material in this article are included in the article's Creative Commons license, unless indicated otherwise in a credit line to the material. If material is not included in the article's Creative Commons license and your intended use is not permitted by statutory regulation or exceeds the permitted use, you will need to obtain permission directly from the copyright holder. To view a copy of this license, visit <http://creativecommons.org/licenses/by/4.0/>.

This is a U.S. Government work and not under copyright protection in the US; foreign copyright protection may apply 2021

# Supplementary Materials for: Expansion of the high field-boosted superconductivity in $\text{UTe}_2$ under pressure

Sheng Ran<sup>1,2,3</sup>, Shanta R. Saha<sup>1,2</sup>, I-Lin Liu<sup>1,2</sup>, David Graf<sup>4</sup>, Johnpierre Paglione<sup>1,2</sup>, Nicholas P. Butch<sup>1,2</sup>

<sup>1</sup> *Maryland Quantum Materials Center, Department of Physics, University of Maryland, College Park, MD 20742, USA*

<sup>2</sup> *NIST Center for Neutron Research,*

*National Institute of Standards and Technology, Gaithersburg, MD 20899, USA*

<sup>3</sup> *Department of Physics, Washington University in St. Louis, St. Louis, MO 63130, USA*

<sup>4</sup> *National High Magnetic Field Laboratory,*

*Florida State University, Tallahassee, FL 32313, USA*

(Dated: July 6, 2021)

## SUPPLEMENTARY NOTES

### Original data of electrical resistance and TDO measurements

In order to clearly present various phases detected by electrical resistance and TDO measurements, color contour plots were shown in the main text. Here we show the original data of electrical resistance and TDO measurements in Fig. 1 and Fig. 3, from which the color contour plots were constructed. The low temperature resistance data is also presented in Fig. 2 for clearance.

### Criterion for determination of the critical magnetic fields

In order to establish phase diagrams unambiguously, we need to introduce a criterion for various critical fields. For superconducting transitions, the critical fields for resistance data are determined as the magnetic fields where the resistance goes to zero and the maximum slope of the resistance data that go to zero resistance. Similarly, the critical fields for TDO data are determined as the magnetic fields where the maximum slope of the TDO data in the superconducting state extrapolate to the TDO data in the normal state. For the metamagnetic transition, the critical field is determined as the peak of  $dR/dH$  in resistance data or the peak of  $df/dH$  in TDO data. The criterion for critical fields of superconducting transitions and metamagnetic transition are presented in Fig. 4, Fig. 5 and Fig. 6.

For the metamagnetic transition, the critical field is determined as the peak of  $dR/dH$  in resistance data or the peak of  $df/dH$  in TDO data. The criterion for metamagnetic critical fields are presented in Fig. 4 and Fig. 5.

We also observed additional features in the field range between the M and  $SC_{FP}$  phases. These anomalies, denoted  $A_{FP}$ , are pronounced in the  $\Delta f$  data, and noticeable in  $R$  data. For TDO data, the lower and upper boundaries of these anomalies are defined as the magnetic fields where the slopes intersect. For  $R$  data, these anomalies are more visible in the derivatives. Therefore, the boundaries of  $A_{FP}$  are defined as local minimums in the derivatives. The criterion for the boundaries of  $A_{FP}$  are shown in Fig. 7.

## Phase diagram at the base temperature

The phase diagram at the base temperature depends on the direction of the magnetic field. In our study, the TDO and resistance measurements were performed at slightly different magnetic field direction. The comparison of the phase diagrams are presented in Fig. 8.

## SUPPLEMENTARY FIGURES

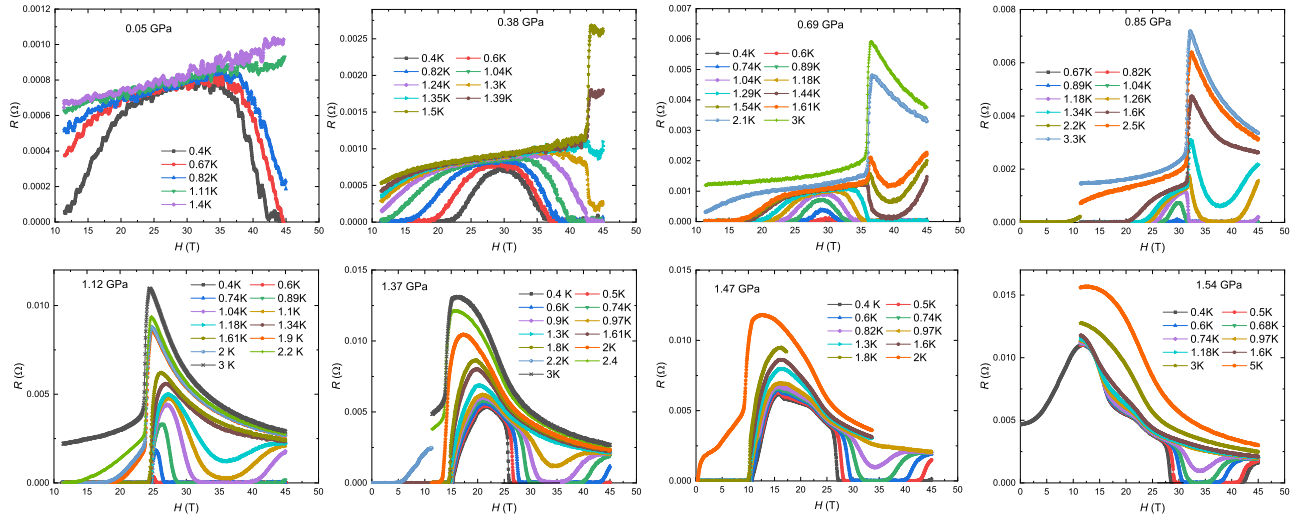


FIG. 1. Field dependence of magnetoresistance of  $UTe_2$  at different temperatures, at pressure values of 0.05, 0.38, 0.69, 0.85, 1.12, 1.37, 1.47, and 1.54 GPa. The magnetic field is applied at 25 degree from  $b$  axis towards  $c$  axis.

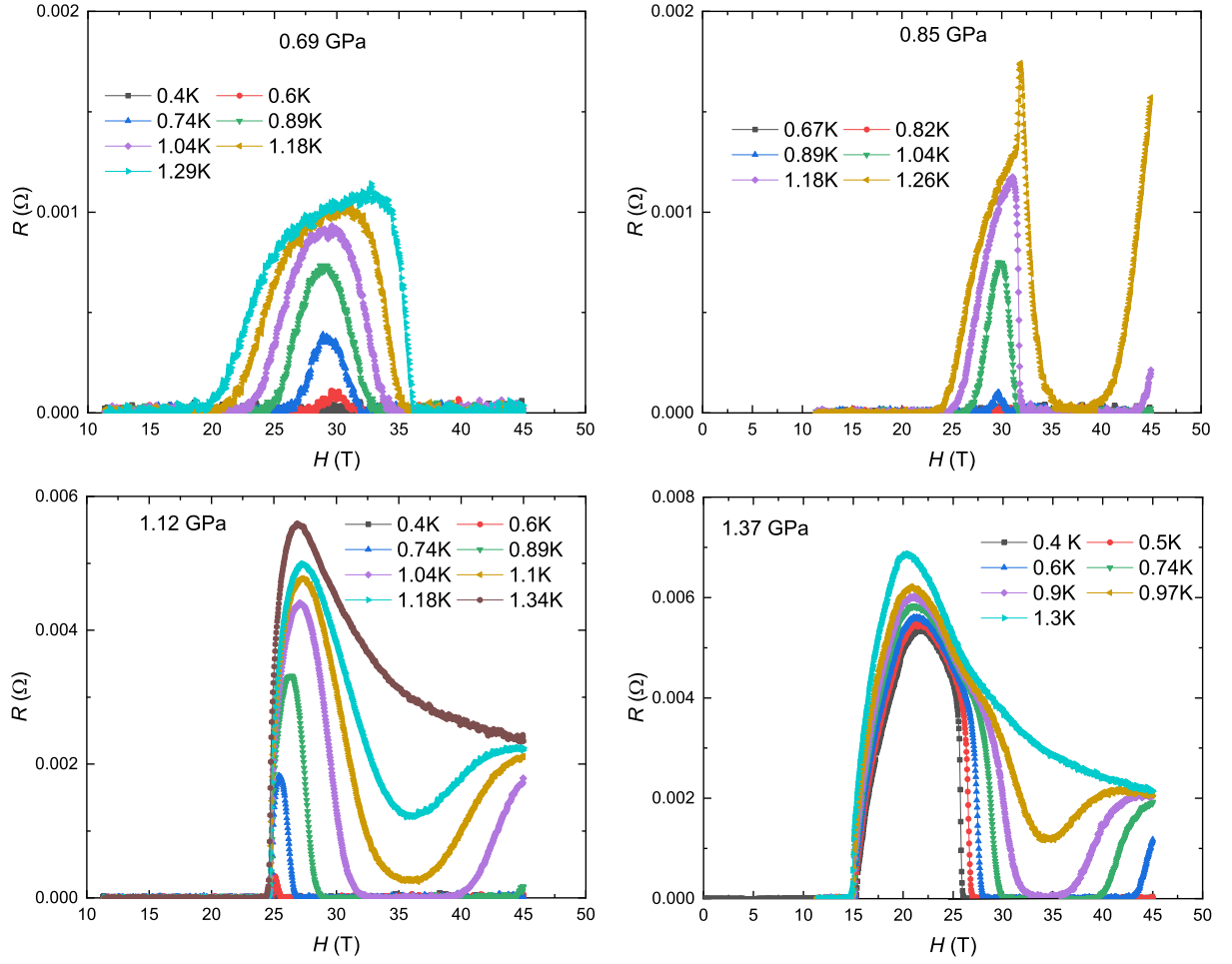


FIG. 2. low temperature field dependence of magnetoresistance of  $\text{UTe}_2$  at different temperatures, at pressure values of 0.05, 0.38, 0.69, 0.85, 1.12, 1.37, 1.47, and 1.54 GPa. The magnetic field is applied at 25 degree from  $b$  axis towards  $c$  axis.

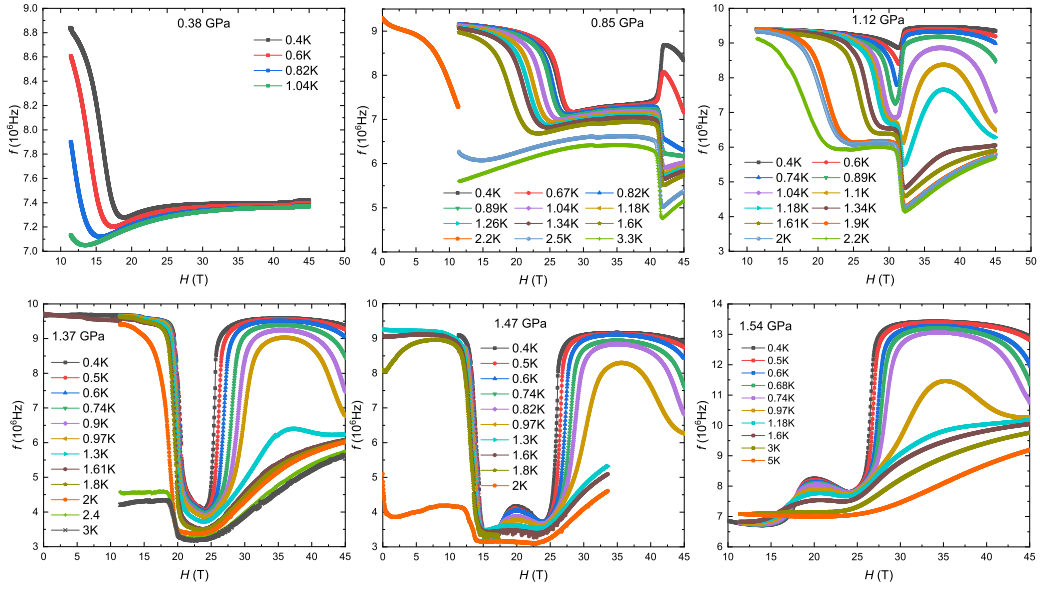


FIG. 3. Field dependence of TDO measurements of  $\text{UTe}_2$  at different temperatures, at pressure values of 0.38, 0.85, 1.12, 1.37, 1.47, and 1.54 GPa. The magnetic field is applied at 30 degree from  $b$  axis towards  $c$  axis.

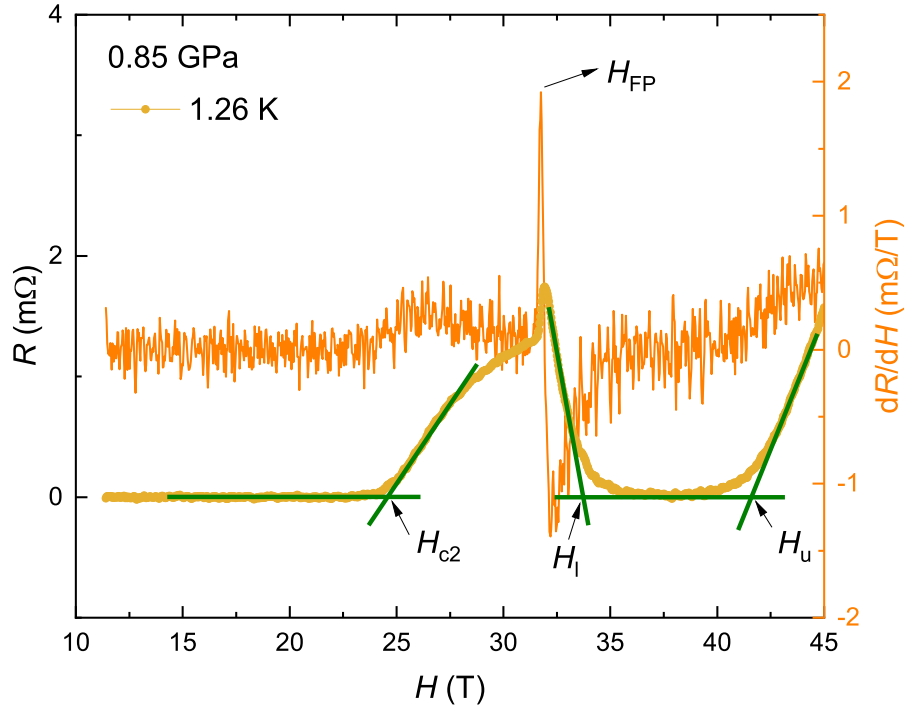


FIG. 4. Criterion for superconducting metamagnetic critical fields from resistance data.

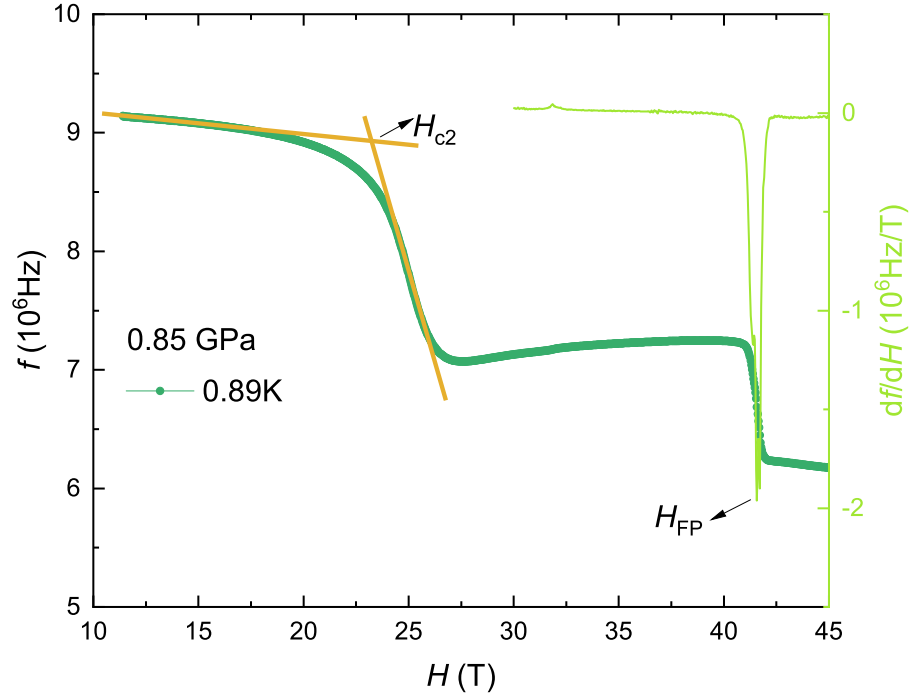


FIG. 5. Criterion for superconducting and metamagnetic critical fields from TDO data.

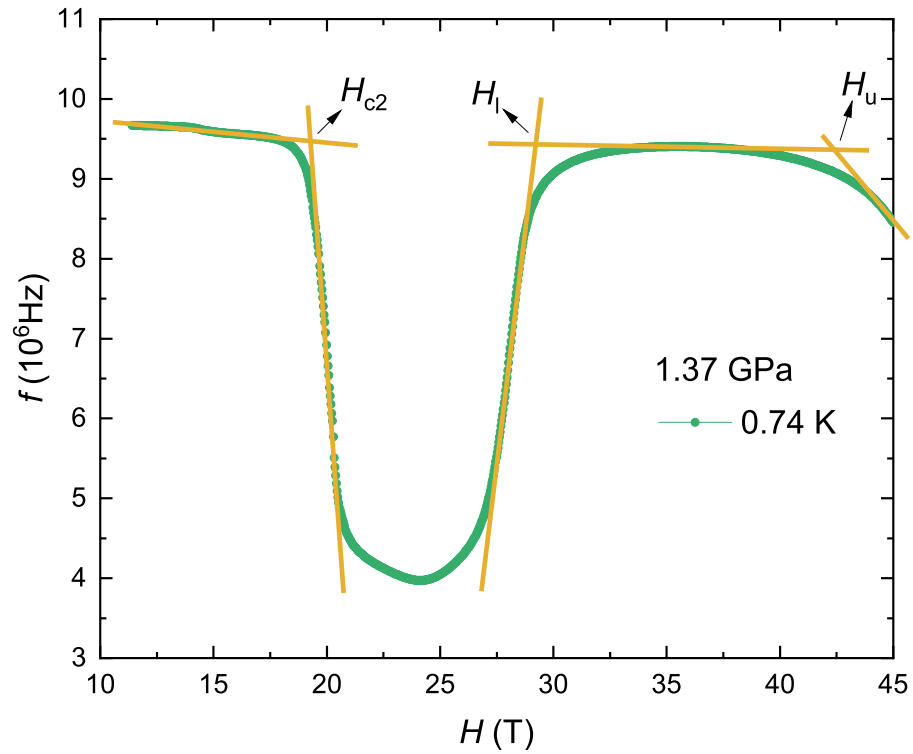


FIG. 6. Criterion for superconducting critical fields from TDO data.

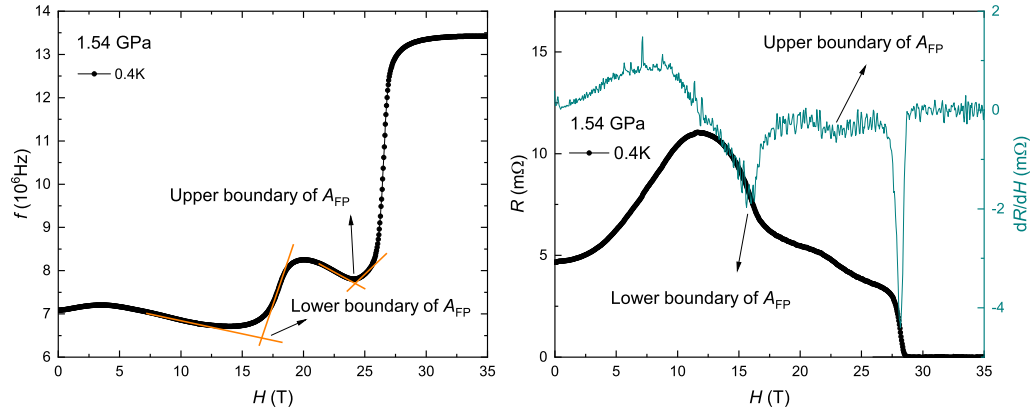


FIG. 7. Criterion for boundaries of the additional features in the field range between the M and  $SC_{FP}$  phases.

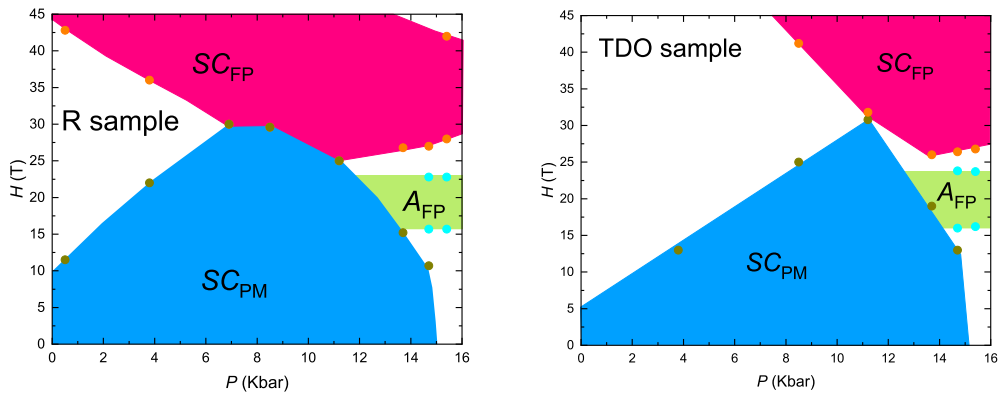


FIG. 8. Phase diagram at the base temperature constructed from resistance and TDO data. For the resistance measurement, the magnetic field is applied at 25 degree from  $b$  axis towards  $c$  axis. For the TDO measurement, the magnetic field is applied at 30 degree from  $b$  axis towards  $c$  axis.